Heliyon 6 (2020) e05529

Contents lists available at ScienceDirect

Heliyon

journal homepage: www.cell.com/heliyon

Research article

Properties of polyacrylamide composites reinforced by cellulose nanocrystals

Marina I. Voronova [a], Oleg V. Surov [a,*], Andrei V. Afineevskii [b], Anatoly G. Zakharov [a]

[a] Laboratory of Physical Chemistry of Polymer-Liquid Heterogeneous Systems, G.A. Krestov Institute of Solution Chemistry of the Russian Academy of Sciences, 1 Akademicheskaya St., Ivanovo 153045, Russian Federation

[b] Department of Physical and Colloid Chemistry, Ivanovo State University of Chemistry and Technology, 7 Sheremetevsky Prospekt, Ivanovo 153000, Russian Federation

ARTICLE INFO

Keywords:
Materials science
Nanotechnology
Cellulose nanocrystals
Polyacrylamide
Polymer composites
Structure-property relationships

ABSTRACT

In this work, a series of polyacrylamide/cellulose nanocrystal (PAM/CNC) composites with a wide range of compositions were prepared by a solution casting method. Subsequently, the influence of the PAM conformation on the behaviour of the PAM/CNC composites was studied. The microstructural, thermal, and mechanical properties of the PAM/CNC composites were also investigated, as well as their flocculation and dispersion behaviour. Thermal degradation of both CNC and PAM in the composites occurred simultaneously, at a much higher temperature than the degradation of the neat CNC. By TEM and SEM, PAM globule aggregates in the PAM/CNC composites were detected. With an increase in the medium acidity, the PAM globule aggregate size of in the composites decreased. Moreover, the composite films cast from high pH solutions (extended PAM conformation) exhibited superior strength properties than those cast from low pH solutions (contracted coil PAM conformation). The PAM globule conformation provided good re-dispersibility of the freeze-dried PAM/CNC composites by preventing aggregation of the CNC particles. The PAM globule adsorption onto the CNC particles caused CNC surface hydrophobization and a decrease in their surface charge, while maintaining high colloidal stability of the CNC suspensions. Furthermore, the CNC particles with adsorbed PAM were demonstrated to be useful as emulsifiers and compatibilisers.

1. Introduction

The high level of technological development of society is increasing the demand for biodegradable household materials (such as containers and packaging) and medical supplies (such as suture materials and implants). Furthermore, it is becoming more and more urgent to solve the environmental problems caused by plastic waste pollution. Regarding these issues, cellulose derivatives have been traditionally used as reinforcing elements for developing biodegradable composites. In recent years, studies of the properties of cellulose nanocrystal (CNC) composites with polymers have made significant contributions to the development of biodegradable and biocompatible materials and functional materials with useful properties.

The last decade has seen a growing interest in CNCs as reinforcing elements due to their renewability, biocompatibility, low density, and high mechanical properties. Generally, CNCs are crystalline rod-like particles with a typical width of 5–20 nm and length between 50–300 nm (Habibi et al., 2010; Klemm et al., 2011; Mondal, 2017; Moon et al., 2011). The surface chemistry, crystallinity, morphology, dimensions, and shape of CNC particles depend both on the hydrolysis conditions and the cellulosic raw material. CNCs can be extracted from cellulose raw sources by different methods such as enzymatic, mechanical, or chemical treatment or their combination. Commonly used inorganic acids preferentially hydrolyse the amorphous parts of cellulose and allow separation of the more resistant crystalline regions.

Currently, CNCs are widely used in smart stimuli-responsive polymer materials, as CNCs can make a unique contribution to the mechanical, optical, and stimuli-responsive properties of the final material (Nasseri et al., 2020). Smart materials can respond to many factors, including mechanical stress, light, or changes in the medium pH or temperature: namely, they possess properties that change reproducibly in response to external stimuli. Subtle changes in the state of smart CNC hybrid systems, such as conformational or volumetric variations in the polymer chain, can result in material macroscopic changes, for instance, stiffening or swelling, solution-to-gel transitions, etc (Salas et al., 2014). Polymer chains constituted of weak polyelectrolytes (e.g., polyacrylamide) are

* Corresponding author.
E-mail address: ovs@isc-ras.ru (O.V. Surov).

https://doi.org/10.1016/j.heliyon.2020.e05529
Received 25 May 2020; Received in revised form 2 September 2020; Accepted 12 November 2020

sensitive to pH changes and reversibly transform from a collapsed globule conformation to an extended chain (Halder et al., 2018). Direct inclusion of CNCs into weak polyelectrolyte polymers that are substantially pH-responsive provides a primary platform for pH sensitivity. By uniting the unique properties of CNC with those of weak polyelectrolyte polymers, it is possible to prepare more advanced, physically adaptable pH-responsive smart systems. Owing to the versatile CNC applications in aqueous suspensions and colloidal systems, CNC-based pH-responsive systems have many potential applications, including pharmaceutics, biomedicine, food engineering, and water treatment (Grishkewich et al., 2017). For instance, the colloidal stability of pH-responsive CNC-based hybrid systems can be controlled by adjusting the hydrophilic/hydrophobic properties of the CNC and tuning pH. This capability enables other applications, such as pH-tuneable flocculation and sedimentation on an industrial scale. Apart from the use in flocculation and sedimentation processes, Pickering emulsions are one of the most significant employments of CNC-based pH-responsive systems (Fujisawa et al., 2017). pH-responsive Pickering emulsifiers based on CNCs have such advantages as better and easier recovery and reusability, eco-compatibility, and low cost. Moreover, in response to pH variations, they may be capable of inducing alternate destabilization/stabilization of the emulsions (Capron et al., 2017).

Polyacrylamide (PAM) is a water-soluble synthetic polymer which possesses useful properties such as good adhesiveness, proper hygroscopicity, high hydrophilicity, and non-toxicity. PAM composites with CNCs can be obtained by mixing an aqueous solution of PAM and an aqueous suspension of CNCs. PAM is a carbochain polymer with a side amide group. Since PAM molecules have $–NH_2$ and –C=O groups, both of which can form hydrogen bonds with the hydroxyl groups of cellulose, we assume an improvement in the thermal and mechanical properties of the resulting PAM/CNC composites. The conformation of a PAM molecule (contraction or expansion) is determined by the surrounding medium pH; namely, the polymer molecule has an extended conformation at a basic pH and a contracted coil conformation at an acidic pH.

Numerous research efforts have been devoted to obtaining composite materials based on PAM and CNCs and studying their properties (Aouada et al., 2011; Chakrabarty and Teramoto, 2018; Spagnol et al., 2012; Yang et al., 2013; Yang et al., 2014; Zhou et al., 2011a,b; Jayaramudu et al., 2019). Most of the reported works were related to the production of PAM/CNC hydrogels. In this case, composite hydrogels were produced during the radical polymerization of acrylamide in the presence of CNC particles. Only a few works reported the fabrication and characterization of CNC-based composite films with PAM as a polymeric matrix (Kurihara and Isogai, 2014; Ryu et al., 2019). pH-responsive CNC-based polymer composites can potentially improve the useful properties of the final functional materials. The importance of these materials stems from the ability of responsive polymers to adopt various conformations (extended, partially extended or coiled), which affects the material macroscopic properties. However, the influence of a polymer molecule conformation on the adsorption behaviour and overall composite properties still remains largely unknown.

In this study, we have formed a series of PAM/CNC composites with a wide range of compositions by a simple and facile casting technique. Additionally, we have investigated the influence of the PAM conformation on the PAM/CNC composite behaviour, and studied the microstructural, thermal and mechanical properties of the PAM composite films reinforced by the CNCs. The specific interactions between the CNCs and PAM in the composites were characterised by FTIR spectroscopy, while the microstructural features of the films were examined by electron microscopy. For thermal properties, the composite films were investigated by thermogravimetric analysis and differential scanning calorimetry, and by tensile testing for mechanical properties. Furthermore, the possibility of using PAM/CNC composites (CNC particles with adsorbed PAM) as emulsifiers was investigated.

2. Materials and methods

2.1. Materials

The microcrystalline cellulose (MCC) (powder, 20 μm), PAM (average Mn 150,000), KBr, sodium chloride, sodium hydroxide, and n-decane were purchased from Sigma-Aldrich (Moscow, Russia). The sulphuric acid (chemically pure) was purchased from Chimmed (Moscow, Russia). Hydrochloric acid (especially pure) was purchased from Sigma-Tech (Moscow, Russia). Throughout the experiment, deionised water was used.,

2.2. Preparation of CNC

The CNCs were obtained from MCC through sulphuric acid hydrolysis, as described in detail earlier (Voronova et al., 2013). According to the transmission electron microscopy (TEM) data, the CNCs were rod-like particles with an average width of 2–4 nm and length of 150–250 nm (an aspect ratio of ~50). The CNC characteristics and TEM image are provided in Table 1 and Figure 1.

2.3. Preparation of PAM/CNC composite films

The composite films were prepared by a solution casting method similar to one described earlier (Voronova et al., 2018). The films obtained were transparent and smooth without any cracks, pores, or cavities.

The composite films of different contents of CNCs (for example, 3 or 9 wt%, etc.) were denoted as PAM/CNC-3, PAM/CNC-9, etc., respectively.

Before testing, all the samples were kept in a desiccator with controlled humidity (75.4 %). The exposure duration was varied from 1 to 5 days, in order for the water content to reach a fixed value of 0.2 g per 1 g of dry sample.

2.4. Preparation of freeze-dried PAM/CNC composites

Freeze-dried samples of the PAM/CNC composites were prepared by freeze-drying aqueous mixtures of the two components. The mixtures of PAM and CNC were sonicated, and then frozen for 48 h at −40 °C and subsequently lyophilised for 36–48 h at −54 °C at a reduced pressure of 6 Pa.

2.5. Characterisation

The tensile properties were measured using an I 1158 M-2.5-01-1 tensile-testing machine (Russia) at room temperature at a loading rate of 2 mm min^{-1} with a solid clamp in the tension mode. Five specimens with the dimensions of 5 mm (width) ×15 mm (length) were used for each sample group. Until testing, all the samples were kept in a desiccator with controlled humidity (75.4 %). The duration of the tensile tests was from 5 to 15 s. Thus, there was a negligible effect of temperature and humidity on the mechanical response of the samples. The strain and stress values were calculated from the machine-recorded displacement and force, based on the original gauge length (10 mm) and the initial cross-sectional area of each sample, respectively. The composite films were about 100 μm thick. Sample thickness was estimated by sampling throughout the sample using a RECXON GY-910 thickness gauge (China) (a measurement accuracy of 3%; a measurement range of 0–1300 μm). Through a linear regression analysis of the initial linear portion of the stress–strain curves, Young's modulus for each sample was calculated. The obtained values of the elongation at break and stress were within ±15%, while the Young's modulus was fluctuated in the range of ±10%.

Differential scanning calorimetric (DSC) measurements were performed on a DSC 204 F1 (Netzsch Gerätebau GmbH, Germany).

Table 1. CNC characteristics.

Parameter	Characteristics
[a]Crystalline dimension by (200) plane, nm	4.4
[a]Crystallinity index, %	86.0
[b]Degree of polymerization	80
[c]Total sulphur content, %	0.66
[d]Zeta-potential, mV	-53
[d]Hydrodynamic diameter, nm	150
[e]Dimensions, nm	
length	150–250
diameter	2–4

[a] X-ray diffraction analysis.
[b] In terms of viscosity of the CNC solution in cadoxene
[c] Elemental analysis.
[d] DLS.
[e] TEM.

Mass spectrometric analysis was performed using an STA 409CD (Netzsch Gerätebau GmbH, Germany) thermo-analytical installation equipped with a QMG 422 skimmer mass-spectroscopic system (In Process Instruments, Germany).

Thermo-gravimetric analysis was performed on a TG 209 F1 (Netzsch Gerätebau GmbH, Germany).

X-ray diffraction (XRD) analysis was performed using a Bruker D8 Advance powder diffractometer (Bruker BioSpin GmbH, Germany) with Cu Kα radiation (λ = 0.1542 nm).

Fourier-transform infrared (FTIR) measurements of the samples were carried out in the range from 4000 to 400 cm^{-1} at room temperature using a VERTEX 80v FTIR spectrometer (Bruker, Germany).

The morphologies of the composites were investigated with a VEGA3 TESCAN scanning electron microscope (Czech Republic).

By measuring the ζ-potential (Zetasizer Nano ZS), the CNC particle surface charge in aqueous suspension was evaluated.

The particle size distributions in the diluted aqueous CNC suspensions were determined by the dynamic light scattering method (DLS) using a Zetasizer Nano ZS (Malvern Instruments Ltd., UK) device.

To determine the dimensions of the CNC particles and PAM globule aggregates, a LEO 912 AB Omega (Carl Zeiss, Germany) TEM (with an accelerating voltage of 100 kV) was used.

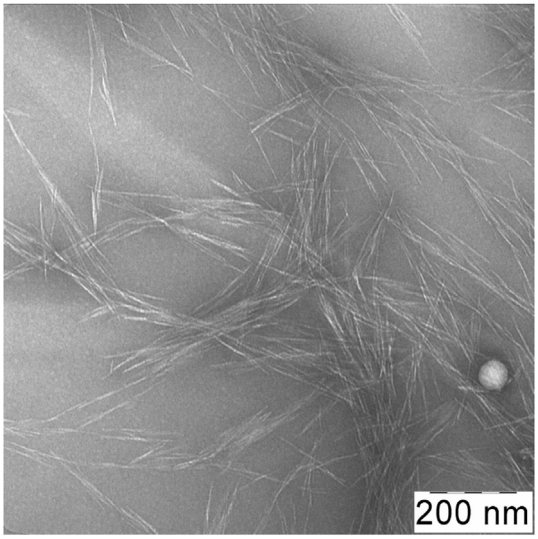

Figure 1. TEM image of CNCs. The scale bar is 200 nm.

3. Results and discussion

3.1. PAM adsorption onto CNC particles

The pH-responsive nature of PAM is through the presence of two functional groups, viz. carbonyl (–C=O) and amine ($–NH_2$). PAM is a weak polyelectrolyte, which means that the net charge of the molecules can be varied as a function of pH. The molecule conformation (i.e., the effective length or shape) is determined by the resulting net charge. At a high pH value (pH > 10), most of the monomers are charged, and the charges result in repulsion among the chain monomer units (the molecule becomes extended). At a low pH value (pH < 4), the carbonyl and amine groups of PAM are undissociated, and the polymer chains tend to have a coiled conformation (Halder et al., 2018). At a pH of 6, PAM molecules adopt a partially extended conformation. Hence, the polymer conformation can be affected by changing the solution pH.

The polymer molecule conformation also depends on the chemical changes in the functional groups due to the interaction with the CNC surface after adsorbing onto the CNC particles. PAM molecules may adsorb onto CNC particles through hydrogen bonding, electrostatic attraction, or hydrophobic interactions. As mentioned above, both of the PAM functional groups (–C=O and $–NH_2$) can form hydrogen bonds with the CNC surface hydroxyl groups.

To interpret the mechanism of PAM interactions with CNC, we have recently carried out classical MD simulations of PAM adsorption onto CNC (Gurina et al., 2020). It was verified that hydrogen bonds are mainly formed via the PAM carbonyl oxygen, and water weakens the interaction between CNC and PAM.

3.2. FTIR analysis

The results of the molecular dynamics simulations of PAM adsorption onto CNC are consistent with the IR spectroscopy data.

For neat PAM, we observed typical bands of stretching vibrations of bonds: N–H at 3440 and 3180 cm^{-1} (symmetric and antisymmetric), C–H at 2920/2850 cm^{-1}, C=O (Amid I) at 1644 cm^{-1}, and C–N in the range of 1460–1400 cm^{-1} (Figure 2) (Ryu et al., 2019).

For neat CNC, we identified the characteristic bands of cellulose. The broad intensive absorption band in the region of 3000–3700 cm^{-1} confirms the stretching vibrations of the cellulose hydroxyl groups participating in hydrogen bonding, wile the C–H bond stretching vibrations in the CH_2 and CH groups are observed in the region of 2800–3000 cm^{-1}.

Since the FTIR spectra of the PAM and cellulose have many overlapping peaks, the characteristic cellulose bands responsible for the stretching vibrations of the pyranose ring (at 1056 and 1034 cm^{-1}), or the bands related to the deformation vibrations of the O–H and C–H bonds (the 'fingerprint' region at 1428, 1380, 1337, and 1318 cm^{-1}) are barely visible on the spectra of the composites, even at a high CNC content. The composite spectra have bands at 1169 and 1118 cm^{-1} (C–O–C and C–C vibrations of the cellulose pyranose ring), but their intensities are low and only weakly dependent on the CNC content in the composite. However, the characteristic bands related to the PAM C=O stretching vibrations shift from 1644 cm^{-1} to larger values at a higher CNC content in the composite films. These results indicate specific hydrogen bonding interactions between the PAM amide groups and the CNC hydroxyl groups.

3.3. X-ray diffraction analysis

The X-ray diffraction patterns of the PAM/CNC films are shown in Figure 3.

The crystalline features of the PAM/CNC composite films were examined with X-ray diffraction patterns (Figure 3). As PAM is an amorphous polymer, the overlapping weaker diffractions close to 14.8° and 16.6° are assigned to the (1–10) and (110) lattice planes of cellulose $I_β$, whereas the diffraction peak arising at about 2θ = 22.9° is attributed

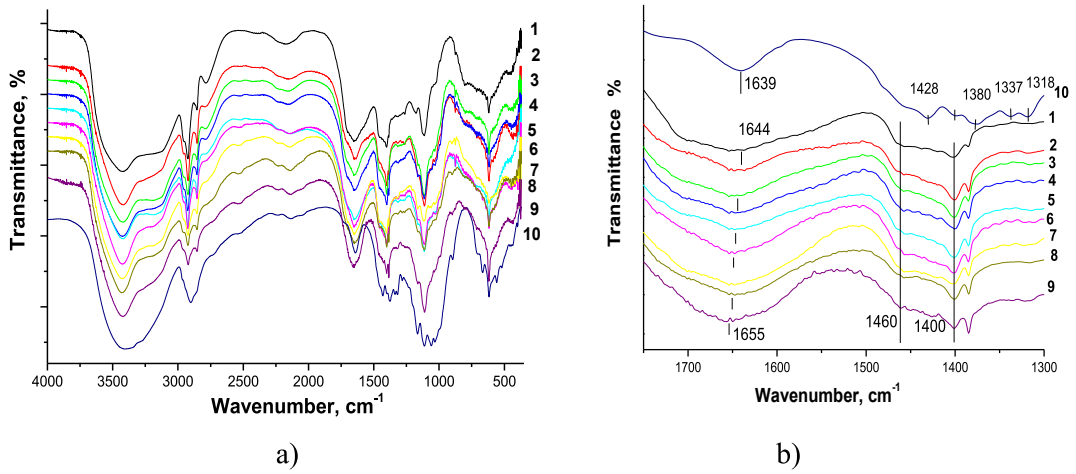

Figure 2. FTIR spectra of the neat PAM (1), neat CNC (10), and PAM/CNC composite films with different CNC content (wt.%): 4.6 (2), 10.3 (3), 15.2 (4), 19.7 (5), 29.8 (6), 40.1 (7), 50.3 (8), and 75.2 (9): (a) in the 4000–500 cm^{-1} range; (b) in the 1700–1300 cm^{-1} range.

to the (200) plane of cellulose I_β (French, 2014). When the CNC content in the composite is increased, the intensity of the diffraction peaks for CNC becomes more pronounced.

3.4. Morphology

The cross-sectional SEM image of the neat PAM film demonstrates some spherical particles (PAM globule aggregates) dispersed in a homogeneous polymer matrix. Moreover, the addition of CNC leads to the appearance of easily distinguishable spherical particles located separately from each other (Figure 4). The spherical particles are observed in the PAM/CNC composites with CNC content of up to 70 wt.%. From the SEM image, it can be seen that the PAM/CNC-70.6 composite has a layered fibrillated structure that is typical of neat CNC.

To estimate the size of the spherical particles in the composites, cross-sectional SEM images of the samples were analysed. A sampling of 100 particles was used to plot a bar chart of particle size distribution (Figure 5). The analysis shows that the average size of the particles decreased with increasing CNC content in the composites, which amounts to 110, 90 and 70 nm for the composites with a CNC content of 4.7, 19.7, and 50.3 wt.%, respectively.

Additionally, we measured the pH values of the solutions from which PAM films and PAM/CNC composite films had been cast. The measured pH values of the solutions were 4.5; 4.2; 3.7, and 3.6 for PAM, PAM/CNC-10, PAM/CNC-30, and PAM/CNC-50, respectively. Thus, with an increase in the CNC content in the composite (i.e., with an increase in the medium acidity), the sizes of the PAM globule aggregates in the composites decreased.

To verify this observation, we cast the PAM films and PAM/CNC composite films from solutions with fixed pH values (Figure 6). The basic and acidic solutions were prepared by adding NaOH to raise the pH and HCl to lower the pH, respectively.

From the results, it can be seen that while PAM globules are most visible in the films cast from solutions with a pH of 6 (the PAM molecules adopt a partially extended conformation), they disappear if the medium acidity increases or decreases (at pH < 3, the contracted PAM globules are too small to be visible, at pH > 10, the PAM molecules have an extended conformation) (Figure 6).

Unfortunately, the SEM micrographs do not allow us to clearly distinguish individual CNCs. Therefore, the CNCs may be adsorbed at the surface of the spherical polymer particles or located between the particles. To provide proof of the CNC spatial distribution within the polymer matrix, we performed TEM observations of a 1:1 aqueous CNC suspension with PAM (PAM/CNC-50 composite).

Unfortunately, individual CNC particles in the composite with PAM are also invisible in the TEM micrographs, apparently, due to the contrast difference between the cellulose and the polymer (Figure 7). However, spherical aggregates consisting of PAM globules are clearly visible. The size of these aggregates is about 100 nm, which is in good agreement with the SEM data.

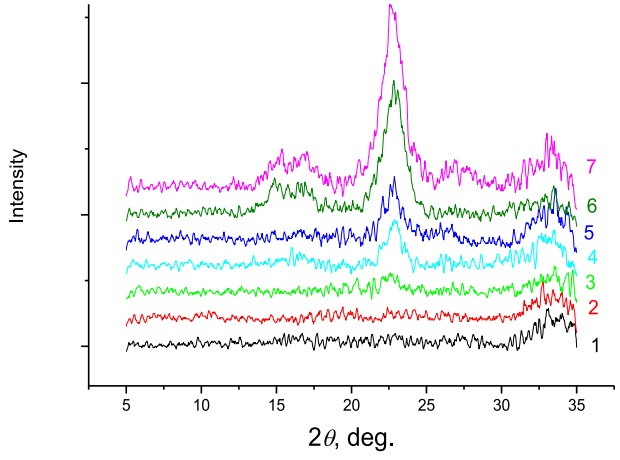

Figure 3. X-ray diffraction patterns of the neat PAM (1) and PAM/CNC composite films with different CNC content (wt.%): 4.6 (2), 10.3 (3), 15.2 (4), 19.7 (5), 29.8 (6), and 40.1 (7).

3.5. Thermal stability

To characterise the thermal stability of the PAM/CNC composites, we carried out thermogravimetric analyses in the temperature range of 25–600 °C. The thermogravimetric (TG) curves and corresponding derivative thermogravimetry (DTG) curves of the PAM/CNC composites are shown in Figure 8, and the appropriate characteristic data are listed in Table 2.

The thermogram obtained for the neat PAM has three main mass loss regions, consistent with some other observations (Leung et al., 1987; Ryu et al., 2019; Tóth et al., 1990; Tutas et al., 1987). The first mass loss region in the range of 25–200 °C is owing to the vaporization of remaining water molecules in the PAM film. The second mass loss in the range of 220–335 °C is caused by the imidisation of the PAM amide group as a result of a cyclisation reaction followed by the removal of the ammonia formed (Kitahara et al., 2012; Tutaş, 1991; Van Dyke and Kasperski, 1993). Two DTG maxima at ~ 235 and 307 °C are observed in this region. The mass spectrometric analysis of the thermal degradation

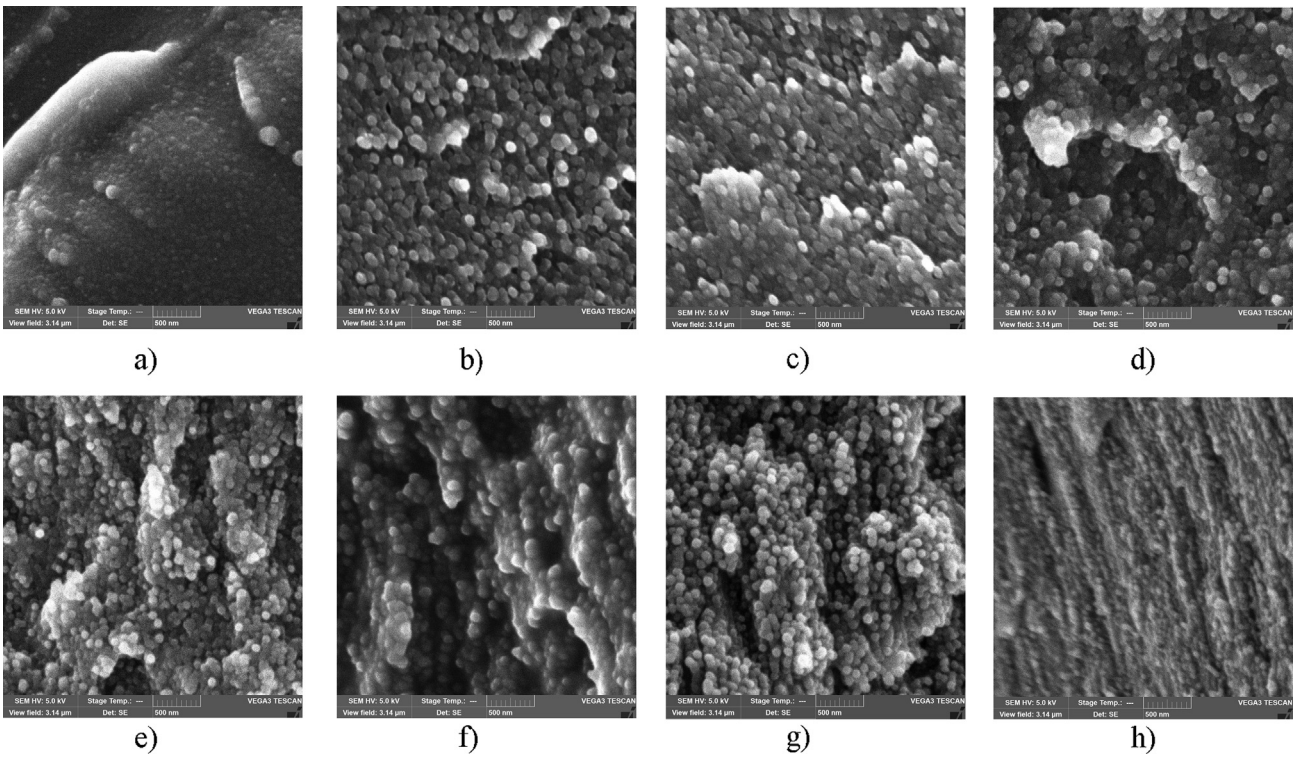

Figure 4. SEM cross section images of the neat PAM film (a) and PAM/CNC composites with different CNC content (wt.%): 4.7 (b), 10.3 (c), 19.7 (d), 29.8 (e), 40.1 (f), 54.5 (g), and 70.6 (h). The scale bar is 500 nm.

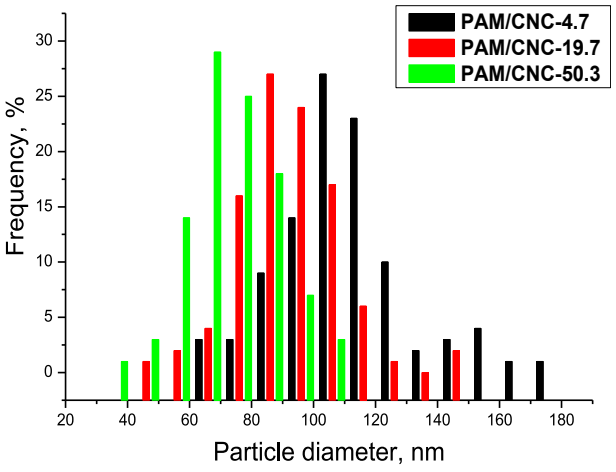

Figure 5. Histograms of particle size distribution for the PAM/CNC composites.

products indicates that the maximum elimination of ammonia occurs at 274 °C (Figure 9a, Table 3). The third mass loss begins at ~ 350 °C and is ascribed to the chain scission of PAM and thermal decomposition of the cyclised imide group. This stage is characterised by the peak degradation temperature at 383 °C and a mass loss of about 60%.

In the PAM/CNC composites, when the CNC content did not exceed 15 wt.%, the CNCs had little effect on the thermal stability of the composites. When the CNC content was above 15 wt.%, new peaks related to the CNC decomposition appeared. With an increase in the CNC content, the thermal stability of the composites decreased. It is well known that the process of sulphuric acid hydrolysis of a cellulosic material for the preparation of CNCs includes an esterification reaction between the acid and the cellulose molecules, which induces covalent coupling of sulphate groups on the surface of the prepared CNCs. Thus, neat CNC show degradation at a much lower temperature (about 200 °C) due to the CNC pyrolysis catalysed by the acid sulphate groups grafted on the CNC surface (Lin and Dufresne, 2014). However, the CNC decomposition temperature in the composites was significantly higher than that of the neat CNC (~200 °C).

The mass spectrometric analysis of the thermal degradation products from the PAM/CNC-19.7 composite (Fig. 9b,d,f, Table 3) indicates that the peak temperatures of the removal of H_2O, NH_3 (T_{max} = 350 °C) and CO_2, SO_2 (T_{max} = 379 °C) are in good agreement with the data of the TG analysis (for the 2nd degradation stage) (Table 2). As CNCs degrade with the formation of SO_2, this suggests that the degradation of both CNC and PAM took place simultaneously at a much higher temperature than degradation of the neat CNC.

3.6. DSC analysis

Before the DSC measurements, all the samples were first equilibrated at -10 °C and heated to 250 °C at a heating rate of 10 K min^{-1}, and then cooled to -10 °C at the same rate. The glass transition temperatures (T_g) for all the samples were determined during the second heating (Figure 10). The results of the DSC analysis of the PAM/CNC films show that when the CNC content was brought to approximately 10–15 wt.%, the T_g of the composites decreased, compared to that of the neat PAM. This behaviour can be related to probable hydrogen bonding interactions between the PAM and CNC, which release the motions of the PAM polymer chains and shift the T_g to a lower temperature region. However, the T_g shifted to higher values when the CNC content in the composites increased. This higher T_g value can indicate that the association of PAM molecules was enhanced by the high CNC content (PAM globule formation). Alternatively, the noticeable increase in the T_g may be ascribed to the macromolecular confinement created by the CNC surfaces (Qin et al.,

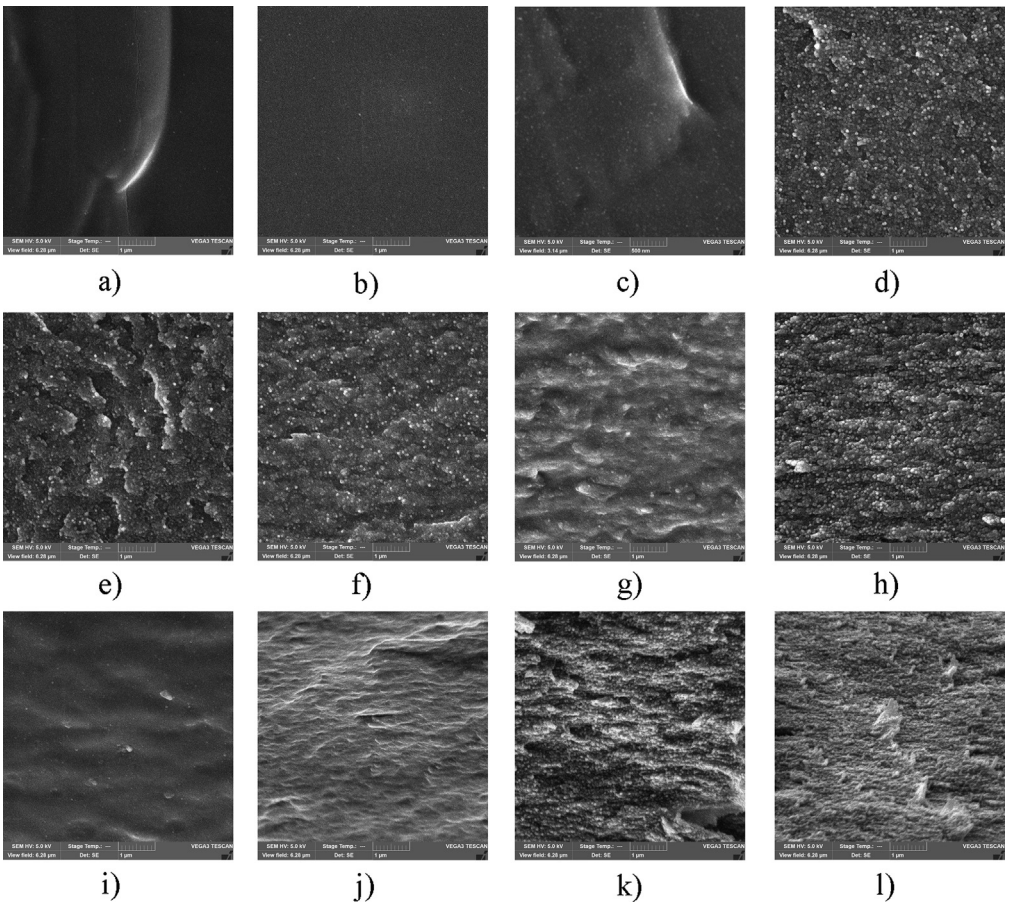

Figure 6. SEM cross section images of the neat PAM films (a–c), and the composite films PAM/CNC-10 (d–f), PAM/CNC-30 (g–i), PAM/CNC-50 (j–l) cast from solutions with pH $\leq$ 3 (left column), pH 6 (middle column), and pH $\geq$ 10 (right column). The scale bar is 1 μm.

2015). Consequently, the nanoconfinement effects may facilitate significant enhancement of the mechanical properties (Surov et al., 2018).

3.7. Mechanical properties

Figure 11 shows stress–strain curves for the PAM/CNC composite films. The values of the Young's modulus (E), elongation at break (ε_b), tensile strength at break (σ_b), and ultimate tensile strength (σ_{max}), are summarized in Table 4. The shapes of the stress-strain curves for the PAM/CNC composites are complex.

At a low CNC content (up to about 10%), the tensile strength of the composite decreased, and the elongation at break increased. With a further increase in the CNC content, the strength characteristics of the composite improved, and the elongation at break decreased. This complex behaviour could be the result of two competing processes. On the one hand, the addition of CNC increased the strength and lowered the elongation at break. On the other hand, an increase in the CNC content in the composite promoted contraction of the polymer macromolecular coils (as the medium acidity increases), which could negatively affect the strength characteristics of the composite. Indeed, the extended chains of the PAM macromolecules interacted more efficiently with each other (due to entanglement effects) and with the CNC particles (due to hydrogen bonds). If PAM macromolecules adopt a globular conformation (at low pH), the compression of the polymer chains would increase the steric repulsive force between the polymer macromolecules, reducing the mechanical properties of the composites. To verify this assumption, we studied the strength characteristics of the PAM films and PAM/CNC composite films which had been cast from solutions with different pH values. The results showed that the films cast from high pH solutions (extended PAM conformation) had superior strength properties to those cast from the low pH solutions (contracted coil PAM conformation) (Table 5).

The analysis of the results obtained shows that the addition of CNCs to the polymer tended to increase the Young's modulus and to reduce the relative elongation of the composites (Table 4). As the CNC content grew, E increased and reached a maximum at the CNC content of ~40 wt.%. However, a further increase in the CNC content resulted in an E decrease. The values of σ_{max} and σ_b also reached their maxima at the ~40 wt.% CNC content. Moreover, the values of the elongation at break, tensile strength at break, and ultimate tensile strength have clear extrema at the CNC content of approximately 10% (the minima for σ_{max} and σ_b and the maximum for ε_b).

The degradation of the composite mechanical properties at a higher CNC content was caused by CNC aggregation. In contrast, Young's modulus increased almost linearly with an increase in the CNC content in the composite, i.e. no percolation threshold was observed. However, the percolation approach suggests strong interactions of CNC particles with each other in a polymer matrix above a percolation threshold (Miao and Hamad, 2019). In our opinion, this circumstance proves that the adsorbed PAM molecules in the PAM/CNC composites complicated the interaction of the CNC particles with each other in the polymer matrix.

3.8. Flocculation and dispersion behaviour of PAM/CNC composites

The sedimentation behaviour of the PAM/CNC composites was influenced by the surrounding media, particularly concerning the

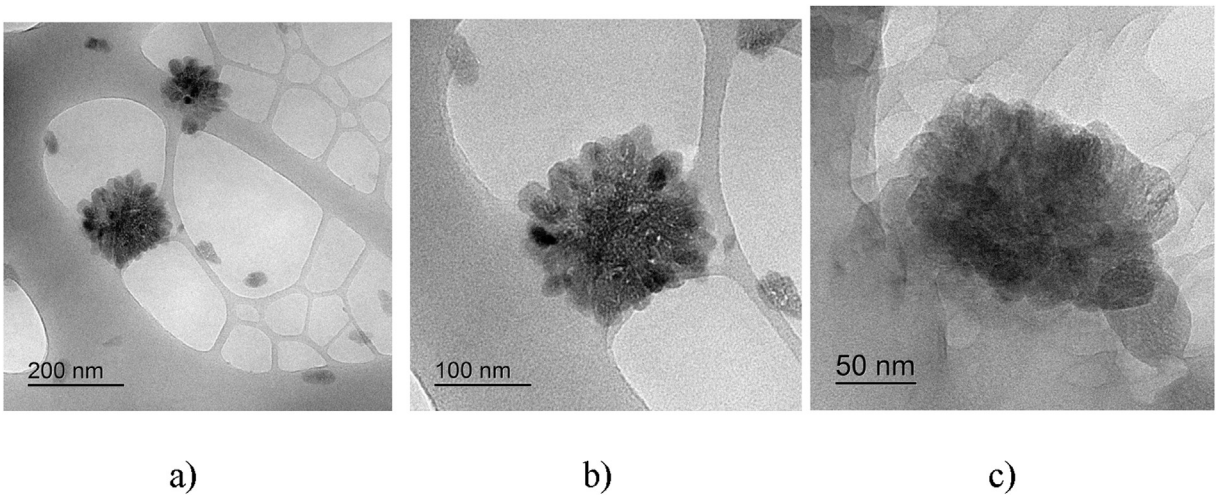

Figure 7. TEM images of PAM/CNC-50 composite. Scales: 200 nm (a); 100 nm (b); 50 nm (c).

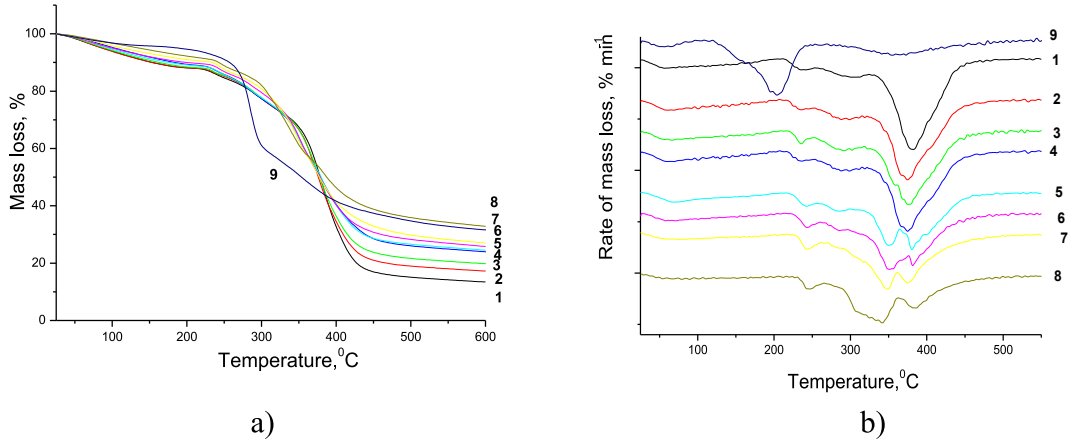

Figure 8. TG (a) and DTG (b) curves of the neat PAM (1), neat CNC (9), and PAM/CNC composite films with different CNC content (wt.%): 4.6 (2), 10.3 (3), 15.2 (4), 19.7 (5), 29.8 (6), 40.1 (7), and 50.3 (8).

Table 2. Thermal stability data for the neat PAM, neat CNC, and PAM/CNC composite films with different CNC content.

Sample	Primary mass loss			1st degradation stage			2nd degradation stage			Entire mass loss, %
	T_{on}, °C	T_{max}, °C	Mass loss, %	T_{on}, °C	T_{max}, °C	Mass loss, %	T_{on}, °C	T_{max}, °C	Mass loss, %	
PAM	-	56	11.9	223.6	235.7	4.0	359.6	382.5	59.5	86.5
					307.0	11.1				
PAM/CNC-4.6	-	68.8	11.9	224.7	236.2	3.2	353.5	374.5	56.1	82.7
					298.8	11.5				
PAM/CNC-10.3	-	66.3	11.8	228.1	235.6	3.1	353.8	375.0	54.4	80.2
					291.8	10.9				
PAM/CNC-15.2	-	70.6	10.9	228.5	237.8	3.4	338.1	352.9	18.7	76.0
					283.0	10.1		381.3	32.9	
PAM/CNC-19.7	-	69.7	11.1	230.8	242.6	4.2	337.1	350.3	19.8	76.1
					286.5	9.1		380.5	31.9	
PAM/CNC-29.8	-	57.8	10.3	234.0	243.4	4.0	334.5	351.5	27.2	74.1
					285.3	5.6		381.4	27.0	
PAM/CNC-40.1	-	70.5	9.5	234.9	243.1	5.3	318.9	348.5	27.8	74.1
					286.1	1.0		374.0	30.5	
PAM/CNC-50.3	-	76.5	8.2	236.9	246.9	4.8	304.8	341.6	29.8	67.2
								385.8	24.4	
CNC	-	58.8	4.3	-	285.5	38.6	-	355.6	26.6	69.5

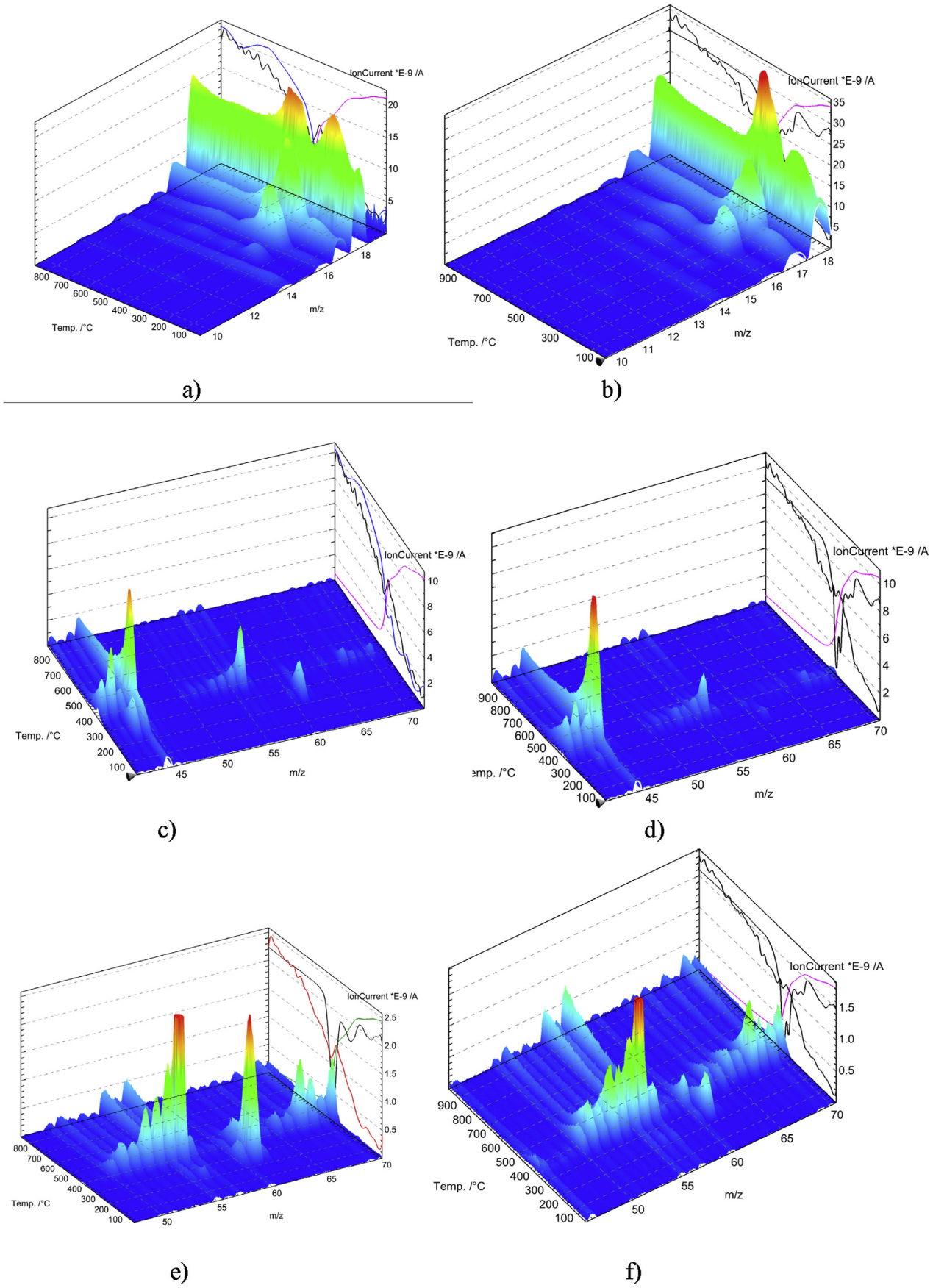

Figure 9. Mass spectra of thermal decomposition products of the neat PAM (a, c, e) and PAM/CNC-19.7 composite (b, d, f) in ranges of various m/z values. The figure also shows the curves of the mass loss and the total ion current (right panels).

Table 3. Thermal degradation products of the neat PAM and PAM/CNC-19.7 composite.

Degradation product	*m/z*	PAM		PAM/CNC-19.7	
		T_{on},°C	T_{max}, °C	T_{on}, °C	T_{max}, °C
NH_3	17	195	274	212	284
				244	350
H_2O	18	25	139	25	145
			309–364	240	350
CO_2	44	195	259	200	254
			379	309	379
SO_2	64	-	-	309	379

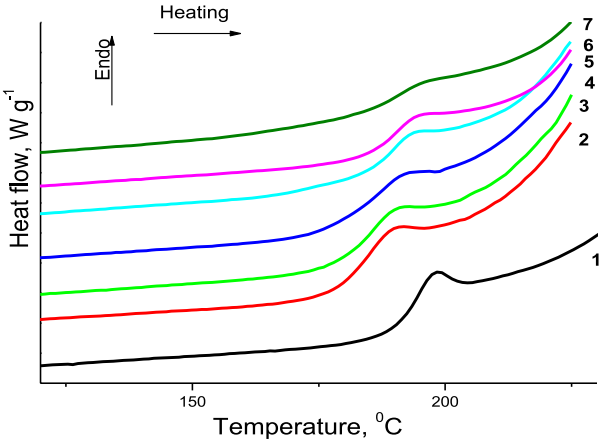

Figure 10. DSC heating traces of the neat PAM (1) and PAM/CNC composite films with various CNC content (wt.%): 4.6 (2), 15.2 (3), 19.7 (4), 29.8 (5), 40.1 (6), and 50.3 (7).

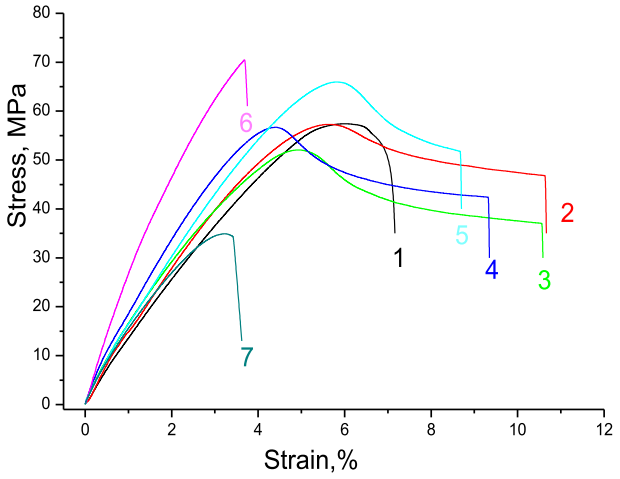

Figure 11. Typical stress–strain curves of the neat PAM (1) and PAM/CNC composite films with different CNC content (wt.%): 4.6 (2), 10.3 (3), 19.7 (4), 29.8 (5), 40.1 (6), and 50.3 (7).

polymer molecular conformations. The flocculation and dispersion behaviours of the PAM/CNC composites were evaluated in terms of the colloidal stability of the suspensions, the surface charge, and the particle-size distribution.

The experimental values of the PAM particle size and ξ-potential obtained by DLS are shown in Figure 12. With an increase in the PAM concentration from 0.05 to 5%, the fraction of the 20 nm particles disappeared, while the percentage of particles of less than 10 nm in size grew. At higher PAM concentrations, the average size of these particles reduced to approximately to 5–6 nm. An increasing concentration reduced the fraction of extended polymer chains, and the degree of coil swelling became lower, which led to coil contraction and a decrease in its size (Figure 12a). The PAM coil contraction was accompanied by an increase in the absolute values of the ξ-potential (Figure 12b).

The PAM adsorption onto the CNC particles was accompanied by growth in the absolute ξ-potential value, and significantly affected the CNC particle size (Figure 13). However, all the PAM/CNC suspensions were stable, no sedimentation was flocculated, and the suspensions retained their good stability even a month later.

Nevertheless, the behaviour of the re-dispersed freeze-dried PAM/CNC composites was quite different (Figure 14).

The re-dispersed aqueous suspensions also demonstrated high colloidal stability after 1 month of storage. Additionally, the particle size of the re-dispersed freeze-dried PAM/CNC composites remained practically unchanged compared to the initial values for the aqueous never-dried CNC (Figure 14a).

Such differences in the behaviour can be explained as follows. A conformation stimuli-response of an adsorbed polymer is not as immediate as the response of the polymer in a solution. The time required for reaching the equilibrium conformation depends on the binding energy between the polymer and the adsorbent surface, the surface coverage, and the polymer molecular weight. Polymer molecules (e.g., molecule train and tail segments) can take a long time to reach the equilibrium conformation (Halder et al., 2018). At the mixing stage, the adsorbed PAM molecules have not yet reached their final conformational state, and the PAM molecules are expected to have a partially extended conformation (pH 4.5). In this case, the PAM molecules may bridge particles via hydrogen bonds at any available free hydroxyl site on the CNC particle surfaces and form aggregates. The bridging occurs (i.e. CNC aggregation), when the extended polymer chains adsorb onto one CNC particle and bind it to other CNC particles. If no bridging is possible (PAM globule conformation at pH $\leq$ 3), the compression of the polymer chain increases the steric repulsive force between the polymer-adsorbed surfaces, preventing aggregation of the CNC particles and providing good re-dispersibility of the freeze-dried PAM/CNC composites.

3.9. PAM/CNC composites as emulsifiers and compatibilisers

It is well known that CNCs can stabilise an oil/water interface due to their surface amphiphilic character (Salas et al., 2014; Capron et al., 2017; Grishkewich et al., 2017). The (200) hydrophobic edge plane is responsible for the CNC wettability at the oil/water interface, and therefore, its accessibility determines the ability to produce stable emulsions. Aqueous suspensions of CNC particles are colloidally stabilised by double-layer repulsive forces due to the surface-grafted sulphate half-ester groups (as a result of controlled hydrolysis with sulphuric acid) that are anionic in most solution conditions. The electrostatic interactions play a major role in the interface control. The CNCs with a high surface charge are not able to efficiently stabilise at the oil/water interface, whereas a decreasing surface charge leads to stable emulsions

Table 4. Tensile properties of the PAM/CNC composite films.

Sample	Young's modulus (E), MPa	Elongation at break (ε_b), %	Tensile strength at break (σ_b), MPa	Ultimate tensile strength (σ_{max}), MPa
PAM	1170	6.5	56.7	56.7
PAM/CNC-4.6	1320	10.6	46.8	57.3
PAM/CNC-10.3	1520	10.5	36.9	52.0
PAM/CNC-19.7	1630	9.3	42.5	56.7
PAM/CNC-29.8	1950	8.7	51.8	66.0
PAM/CNC-40.1	2740	3.7	70.4	70.4
PAM/CNC-50.3	1380	3.4	34.5	34.5

Table 5. Tensile properties of the PAM/CNC composite films cast from the solutions with different pH values.

Sample	Young's modulus (E), MPa	Elongation at break (ε_b), %	Tensile strength at break (σ_b), MPa	Ultimate tensile strength (σ_{max}), MPa
PAM				
pH 2.5	1090	7.2	46.6	48.8
pH 6.5	1440	6.2	52.8	59.9
pH 10.0	1230	6.5	57.2	62.9
PAM/CNC-10.3				
pH 2.2	1140	3.8	33.4	33.4
pH 6.2	1770	9.5	38.9	54.4
pH 10.0	2050	8.8	41.0	57.2
PAM/CNC-29.8				
pH 1.8	570	2.9	30.6	30.6
pH 6.0	2140	7.3	58.8	72.6
pH 10.0	2100	6.3	55.4	66.0
PAM/CNC-50.3				
pH 2.0	840	0.6	5.1	5.1
pH 6.1	1510	2.1	31.1	31.1
pH 10.0	1710	1.9	33.4	33.4

(Kalashnikova et al. 2012). This wetting change can be managed by screening the charge repulsions, for example, by means of changing the pH, the ionic strength of a solution, or polymer adsorption.

To model an oil/water interface, we prepared n-decane/water emulsions. The prepared decane-in-water Pickering emulsions stabilized by PAM/CNC composites (1:1 ratio) had a constant n-decane:water ratio of 2:8 (Figure 15). The aqueous phase consisted of aqueous CNC suspensions (1 wt.% concentration) with PAM, at different pH values and with an NaCl addition. Pure water, a PAM solution, and a CNC suspension were used to compare the emulsification properties. The mixtures of decane and aqueous suspensions were sonicated twice for 5 min with a 5 min delay (Sonorex DT 100 Bandelin, Germany).

Figure 15 shows that sonication yields creaming with the formation of a stable emulsion, only for the PAM/CNC composite at pH 3 (sample 8). The long-term stability of the emulsions without flocculation and coalescence was determined by visual inspection a month after the preparation.

At low and high pH values, CNCs may have a lower charge and be slightly aggregated due to reduced double-layer repulsion when the surface sulphate ester groups are protonated (pH $<$ 3), or if some desulphation occurs in strongly basic conditions (pH $>$ 10) (Zhong et al., 2012). Moreover, if the ionic strength is high enough, a charge screening effect may be quite noticeable and lead to particle aggregation. These effects were especially pronounced in the presence of PAM (turbid

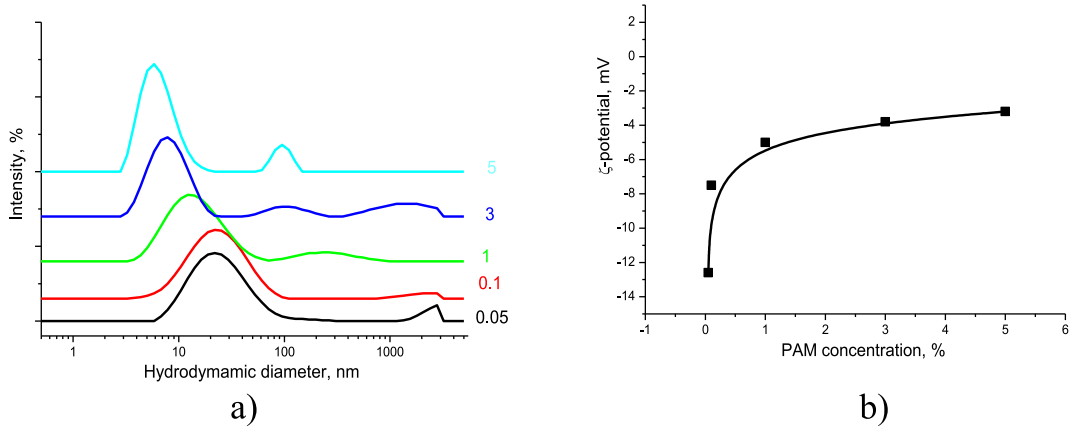

Figure 12. PAM particle size distribution (the curves are marked by PAM concentration in wt.%) (a) and PAM particle surface charge in the aqueous solutions (b).

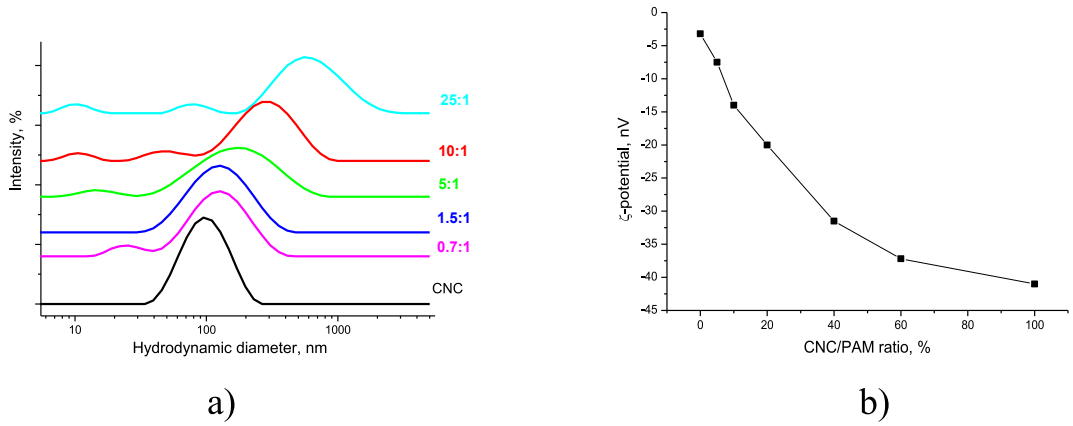

Figure 13. CNC particle size distribution in the presence of PAM (the curves are marked by the PAM/CNC concentration ratio) (a) and CNC particle surface charge in aqueous suspensions (CNC concentration of 0.07 wt.%) in the presence of PAM (b).

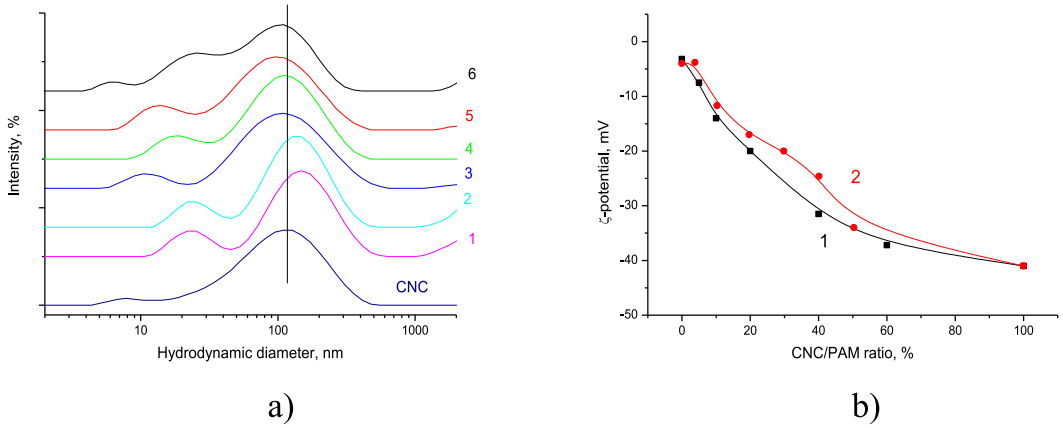

Figure 14. Particle size distribution of re-dispersed freeze-dried PAM/CNC composites in water with different CNC content (wt.%) (the neat CNC curve is shown for comparison): 50.3 (1), 40.1 (2), 29.8 (3), 19.7 (4), 10.3 (5), and 4.6 (6) (a); CNC particle surface charge in aqueous suspensions (CNC concentration of 0.07 wt.%) in the presence of PAM (1) and particle surface charge of the freeze-dried PAM/CNC composites after re-dispersion in water (2) (b).

suspensions were observed) due to intermolecular bridging interactions or entanglement (Figure 11, samples 6 and 7). However, at a pH of 3, the CNC surface with adsorbed PAM must become more hydrophobic due to the PAM contracted-coil conformation. Moreover, as a PAM molecule contains a large hydrophobic alkyl group, the adsorbed PAM molecules prevented CNC nanoparticles aggregation through repulsive forces arising from the hydrophobic carbon chains. Thus, the PAM adsorption onto CNC at a pH of 3 caused the CNC surface hydrophobization and a decrease in the surface charge (due to the screening of the underlying CNC surface charge) while maintaining the high colloidal stability of the CNC suspensions. These conditions make it possible to obtain stable oil-in-water Pickering emulsions.

By virtue of their highly hydrophilic behaviour, CNCs may not be uniformly distributed in a hydrophobic polymer matrix, resulting in poor interfacial adhesion and agglomeration, and poor final properties of the bio-composites. In this respect, the use of an amphiphilic compatibiliser, such as PAM, can overcome these problems due to its water solubility, nontoxicity, biodegradability, and biocompatibility (Singh et al., 2020). The specific application of such a system could include effective production methods of polymer composites with high CNC

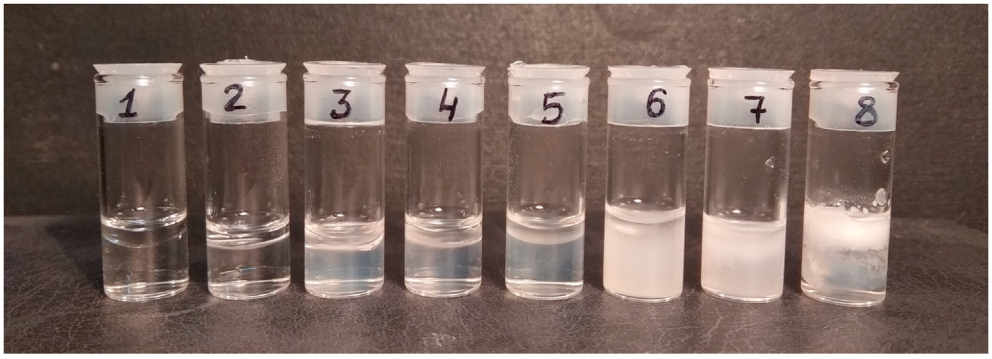

Figure 15. Photos of the aqueous emulsions with n-decane: 1 - water; 2 - PAM; 3 - CNC; 4 - PAM/CNC (1:1 ratio); 5 - PAM/CNC (pH 6); 6 - PAM/CNC (pH 10); 7 - PAM/CNC (pH 3.6, C_{NaCl} = 0.05 mol L^{-1}); 8 - PAM/CNC (pH 3).

content, with further applicability in the plastic industry (cutlery, disposable containers, packaging, and so on). However, this topic is well beyond the aim of the present research and is a purpose for our further investigation.

4. Conclusions

In this work, pH-responsive PAM/CNC composites were prepared by a solution casting method. Our subsequent investigation and analysis determined that the PAM ability to adopt various conformations at different pH values impacts the macroscopic properties of the composite material. Therefore, the influence of the PAM conformation on the PAM/CNC composite behaviour was studied, and the microstructural, thermal and mechanical properties of the PAM/CNC composites were also evaluated. Furthermore, the use of PAM/CNC composites (CNC particles with adsorbed PAM) as emulsifiers and compatibilisers has been demonstrated.

Declarations

Author contribution statement

Marina I. Voronova, Andrei V. Afineevskii: Conceived and designed the experiments; Performed the experiments; Analyzed and interpreted the data.

Oleg V. Surov: Conceived and designed the experiments; Performed the experiments; Analyzed and interpreted the data; Wrote the paper.

Anatoly G. Zakharov: Conceived and designed the experiments; Analyzed and interpreted the data; Contributed reagents, materials, analysis tools or data.

Funding statement

This work was supported by the Russian Science Foundation (17-13-01240 П).

Data availability statement

Data included in article/supplementary material/referenced in article.

Declaration of interests statement

The authors declare no conflict of interest.

Additional information

No additional information is available for this paper.

Acknowledgements

The authors would like to thank the Centre for Collective Use of Scientific Equipment of Ivanovo State University of Chemistry and Technology (Russia) and the Upper Volga Region Centre of Physico-chemical Research (Ivanovo, Russia) for some measurements taken with the use of their equipment.

References

Aouada, F.A., de Moura, M.R., Orts, W.J., Mattoso, L.H., 2011. Preparation and characterization of Novel micro- and nanocomposite hydrogels containing cellulosic fibrils. J. Agric. Food Chem. 59, 9433–9442.

Capron, I., Rojas, O.J., Bordes, R., 2017. Behavior of nanocelluloses at interfaces. Curr. Opin. Colloid In 29, 83–95.

Chakrabarty, A., Teramoto, Y., 2018. Recent advances in nanocellulose composites with polymers: a guide for choosing partners and how to incorporate them. Polym.-Basel 10, 517.

French, A.D., 2014. Idealized powder diffraction patterns for cellulose polymorphs. Cellulose 21 (2), 885–896.

Fujisawa, S., Togawa, E., Kuroda, K., 2017. Nanocellulose-stabilized Pickering emulsions and their applications. Sci. Technol. Adv. Mater. 18 (1), 959–971.

Grishkewich, N., Mohammed, N., Tang, J., Tam, K.C., 2017. Recent advances in the application of cellulose nanocrystals. Curr. Opin. Colloid In. 29, 32–45.

Gurina, D., Surov, O., Voronova, M., Zakharov, A., 2020. Molecular dynamics simulation of polyacrylamide adsorption on cellulose nanocrystals. Nanomaterials-Basel 10, 1256.

Habibi, Y., Lucia, L.A., Rojas, O.J., 2010. Cellulose nanocrystals: chemistry, self-assembly, and applications. Chem. Rev. 110, 3479–3500.

Halder, B.K., Palomino, A.M., Hicks, J., 2018. Influence of polyacrylamide conformation on fabric of "tunable" kaolin–polymer composite. Can. Geotech. J. 55 (9), 1295–1312.

Jayaramudu, T., Ko, H.-U., Kim, H.C., Kim, J.W., Kim, J., 2019. Swelling behavior of polyacrylamide–cellulose nanocrystal hydrogels: swelling kinetics, temperature, and pH effects. Materials 12, 2080.

Kalashnikova, I., Bizot, H., Cathala, B., Capron, I., 2012. Modulation of cellulose nanocrystals amphiphilic properties to stabilize oil/water interface. Biomacromolecules 13, 267–275.

Kitahara, Y., Okuyama, K., Ozawa, K., Suga, T., Takahashi, S., Fujii, T., 2012. Thermal decomposition of acrylamide from polyacrylamide. Time-resolved pyrolysis with ion-attachment mass spectrometry. J. Therm. Anal. Calorim. 110, 423–429.

Klemm, D., Kramer, F., Moritz, S., Lindström, T., Ankerfors, M., Gray, D., Dorris, A., 2011. Nanocelluloses: a new family of nature-based materials. Angew. Chem. Int. Ed. 50, 5438–5466.

Kurihara, T., Isogai, A., 2014. Properties of poly(acrylamide)/TEMPO-oxidized cellulosenanofibril composite films. Cellulose 21, 291–299.

Leung, W.M., Axelson, D.E., Van Dyke, J.D., 1987. Thermal degradation of polyacrylamide and poly(acrylamide-co-acrylate). J. Polym. Sci. A1 (25), 1825–1846.

Lin, N., Dufresne, A., 2014. Surface chemistry, morphological analysis and properties of cellulose nanocrystals with gradiented sulfation degrees. Nanoscale 10, 5384–5393.

Miao, C., Hamad, W.Y., 2019. Critical insights into the reinforcement potential of cellulose nanocrystals in polymer nanocomposites. Curr. Opin. Solid St. M. 23, 100761.

Mondal, S., 2017. Preparation, properties and applications of nanocellulosic materials. Carbohydr. Polym. 163, 301–316.

Moon, R.J., Martini, A., Nairn, J., Simonsen, J., Youngblood, J., 2011. Cellulose nanomaterials review: structure, properties and nanocomposites. Chem. Soc. Rev. 40, 3941–3994.

Nasseri, R., Deutschman, C.P., Han, L., Pope, M.A., Tam, K.C., 2020. Cellulose nanocrystals in smart and stimuli-responsive materials: a review. Mater. Today Adv. 5, 100055.

Qin, X., Xia, W., Sinko, R., Keten, S., 2015. Tuning glass transition in polymer nanocomposites with functionalized cellulose nanocrystals through nanoconfinement. Nano Lett. 15, 6738–6744.

Ryu, J.H., Han, N.K., Lee, J.S., Jeong, Y.G., 2019. Microstructure, thermal and mechanical properties of composite films based on carboxymethylated nanocellulose and polyacrylamide. Carbohydr. Polym. 211, 84–90.

Salas, C., Nypelö, T., Rodriguez-Abreu, C., Carrillo, C., Rojas, O.J., 2014. Nanocellulose properties and applications in colloids and interfaces. Curr. Opin. Colloid In 19, 383–396.

Singh, A.A., Genovese, M.E., Mancini, G., Marini, L., Athanassiou, A., 2020. Green processing route for polylactic Acid−Cellulose fiber biocomposites. ACS Sustain. Chem. Eng. 8, 4128–4136.

Spagnol, C., Rodrigues, F.H.A., Neto, A.G.V.C., Pereira, A.G.B., Fajardo, A.R., Radovanovic, E., Rubira, A.F., Muniz, E.C., 2012. Nanocomposites based on poly(acrylamide-co-acrylate) and cellulose Nanowhiskers. Eur. Polym. J. 48, 454–463.

Surov, O.V., Voronova, M.I., Afineevskii, A.V., Zakharov, A.G., 2018. Polyethylene oxide films reinforced by cellulose nanocrystals: microstructure-properties relationship. Carbohydr. Polym. 181, 489–498.

Tóth, I., Szépvölgyi, J., Jakab, E., Szabó, P., Székely, T., 1990. Thermal decomposition of a bentonite-polyacrylamide complex. Thermochim. Acta 170, 155–166.

Tutaş, M., 1991. Investigation of pyrolysis products of polyacrylamide by pyrolysis-gas chromatography. J. Anal. Appl. Pyrol. 22, 129–137.

Tutas, M., Sağlam, M., Yüksel, M., Güler, Ç., 1987. Investigation of the thermal decomposition kinetics of polyacrylamide using a dynamic TG technique. Thermochim. Acta 111, 121–126.

Van Dyke, J.D., Kasperski, K.L., 1993. Thermogravimetric study of polyacrylamide with evolved gas analysis. J. Polym. Sci. 31, 1807–1823.

Voronova, M.I., Surov, O.V., Zakharov, A.G., 2013. Nanocrystalline cellulose with various contents of sulfate groups. Carbohydr. Polym. 98 (1), 465–469.

Voronova, M., Rubleva, N., Kochkina, N., Afineevskii, A., Zakharov, A., Surov, O., 2018. Preparation and characterization of polyvinylpyrrolidone/cellulose nanocrystals composites. Nanomaterials-Basel 8, 1011.

Yang, J., Han, C.-R., Duan, J.-F., Ma, M.-G., Zhang, X.-M., Xu, F., Sun, R.-C., 2013. Synthesis and characterization of mechanically flexible and tough cellulose nanocrystals–polyacrylamide nanocomposite hydrogels. Cellulose 20, 227–237.

Yang, J., Zhao, J.-J., Zhang, X.-M., 2014. Modification of cellulose nanocrystal-reinforced composite hydrogels: effects of co-crosslinked and drying treatment. Cellulose 21, 3487–3496.

Zhong, L., Fu, S., Peng, X., Zhan, H., Sun, R., 2012. Colloidal stability of negatively charged cellulose nanocrystalline in aqueous systems. Carbohydr. Polym. 90, 644–649.

Zhou, C., Wu, Q., Yue, Y., Zhang, Q., 2011a. Application of rod-shaped cellulose nanocrystals in polyacrylamide hydrogels. J. Colloid Interface Sci. 353, 116–123.

Zhou, C., Wu, Q., Zhang, Q., 2011b. Dynamic rheology studies of in situ polymerization process of polyacrylamide–cellulose nanocrystal composite hydrogels. Colloid Polym. Sci. 289, 247–255.